Journal of Alloys and Compounds 826 (2020) 153977

Contents lists available at ScienceDirect

Journal of Alloys and Compounds

journal homepage: http://www.elsevier.com/locate/jalcom

Unique hybrid precipitate structures forming in an Al–Cu–Mg–Si alloy

Marat Gazizov [a, *], Calin Daniel Marioara [b], Jesper Friis [b, c], Sigurd Wenner [b, c], Randi Holmestad [c], Rustam Kaibyshev [a]

[a] Belgorod State University, 308015, Belgorod, Russia
[b] Materials and Nanotechnology, SINTEF Industry, N-7465, Trondheim, Norway
[c] Department of Physics, Norwegian University of Science and Technology (NTNU), N-7491, Trondheim, Norway

ARTICLE INFO

Article history:
Received 11 September 2019
Received in revised form
14 January 2020
Accepted 20 January 2020
Available online 31 January 2020

Keywords:
Metals and alloys
Atomic scale structure
Transmission electron microscopy
TEM
Computer simulations

ABSTRACT

Crystal structures of hybrid precipitates have been analysed by atomic-resolution scanning transmission electron microscopy in an aged Al–Cu–Mg–Si alloy. A new unique hybrid precipitate (UHP) has been found as rod-shaped discrete particles along $\langle 100 \rangle_{Al}$ in bulk aluminium matrix. The UHP consists of a core with local 4-fold symmetry surrounded by GPB zone unit pillars often combined with monoatomic Cu layers in fcc-Al matrix. A certain atomic configuration fragment of the UHP structure is often seen to inter-grow with other hybrid precipitate complexes consisting of diverse phases belonging to the Al–Cu–Mg–Si and Al–Cu alloy systems. Density functional theory (DFT) calculations performed on a discrete UHP showed that the most energetically favorable core configuration resembles a β″-eye from the Al–Mg–Si system rotated 45 °C in respect to its usual orientation with the fcc-Al matrix.

© 2020 Elsevier B.V. All rights reserved.

1. Introduction

Commercial aluminium alloys based on the Al–Cu system are used as structural materials for aircraft and automotive applications due to a combination of desirable properties like high specific strength (strength/weight ratio), good formability and high fracture toughness, often combined with satisfactory corrosion resistance [1–3]. The maximum service strength of theses alloys is reached during ageing at elevated temperatures due to formation of nano-scale particles. A further improvement in mechanical properties can be achieved by additions of Mg and Si [4]. In this case the precipitates formed during ageing are a complex mix of phases from the Al–Mg–Si(-Cu), Al–Cu–Mg and Al–Cu systems. It was recently shown that many of such precipitates are not single-phase, but hybrid structures that include fragments of various phases from the above-mentioned systems in the same precipitate [2,4,5]. In general, the precipitation sequence in a bulk matrix during aging of Al–Cu–Mg–Si alloys can be written as [2,5]:

$$\begin{aligned} &SSSS \rightarrow clusters \rightarrow \\ &\rightarrow GP + GPB + \theta'' + \beta'' + \beta' - Cu + C + \theta' + Q' \rightarrow \\ &\rightarrow GPB + \theta' + C + Q' \end{aligned} \quad (1)$$

where GP are Guinier-Preston zones determined as mono-atomic $\{100\}_{Al}$ layers of Cu in Al–Cu–Mg–Si alloys [5,6]; GPB are Guinier-Preston-Bagaryatsky zones (or zone units) determined as nanometer-scale $\langle 100 \rangle_{Al}$ rod-shaped agglomerates of Al, Cu and Mg columns in Al–Cu–Mg alloys [7,8]. Chemical composition, crystal structure, morphology and orientation relationships of the GP and GPB zones, θ″, θ′, β″, β′-Cu, C, and Q′-phases have been discussed in detail previously [3–14]. Knowledge about organization of these structures is important in order to better understand the precipitation phenomenon in multiphase Al–Cu–Mg–Si alloys.

Complex analysis of atomic resolution TEM images (usually taken in different crystal zone axes (ZA)) combined with density functional theory (DFT) calculations is required to verify atomic models suggested for the observed precipitate structures. Andersen et al. [15] applied this approach and discovered phase construction rules for precipitates in Al–Mg–Si-(Cu) and Al–Mg–Cu alloys, where annular dark-field (S)TEM (ADF-STEM) was used for imaging

* Corresponding author.
E-mail addresses: gazizov@bsu.edu.ru (M. Gazizov), Calin.D.Marioara@sintef.no (C.D. Marioara), Jesper.Friis@sintef.no (J. Friis), Sigurd.Wenner@ntnu.no (S. Wenner), Randi.Holmestad@ntnu.no (R. Holmestad), Rustam_Kaibyshev@bsu.edu.ru (R. Kaibyshev).

https://doi.org/10.1016/j.jallcom.2020.153977
0925-8388/© 2020 Elsevier B.V. All rights reserved.

in $\{200\}_{Al}$ projection planes. According to these rules, every Al atom has 12 nearest neighbors (NNs), every Mg atom has 15 and every Si has 9. It means that in the $\{200\}_{Al}$ projection plane every Al, Mg and Si atomic column is surrounded by 4, 5 and 3 columns having 'opposite' height (±0.203 nm), respectively. Cu atomic columns show local 3-fold symmetry (as Si) if located inside the precipitates or GPB zones, and take Al column configuration at the precipitate interfaces with the Al matrix, or if part of GP zones and θ″-phase [5,15,16]. This method is useful and easily applicable to identify the atomic column arrangement in the extend cross-sections of hybrid precipitates, when atomic column distribution periodicity exists (for example, apparent Si- and Cu-networks in the ADF-STEM images of the cross-section projections for the precipitates in Al—Mg—Si—Cu alloys or only Cu-network in precipitates in Al—Cu(-Mg) alloys) [5,14–16].

Recently we used ADF-STEM images and phase construction rules to identify the fragments of different phases in hybrid precipitate complexes forming in the Al—Cu—Mg—Si alloy during aging [5]. DFT calculations for a few suggested structures showed that Cu segregation at interfaces between different hybrid precipitates and the Al matrix is required to make them energetically favorable. GPB units were also found at that interfaces in under-, peak- and over-aging stages, despite their metastable nature in Al—Cu—Mg alloys [5].

In this work, we present TEM observations of phase fragments forming UHPs and consisting of a certain atomic column arrangement of Mg and Si in a transitional layer between fcc-Al matrix and GPB zone unit pillars or GP-like structures (monoatomic Cu layer in the fcc-Al matrix). The phase construction rules have been applied to suggest several variants of possible atomic column arrangements for these UHP fragments. DFT calculations were used to understand important structural observations and find out a most energetically favorable case for the discrete rod-like UHPs.

2. Experimental procedure

2.1. Sample preparation

The investigated alloy has a nominal composition of Al-4.9Cu-0.74Mg-0.51Si-0.48Mn-0.1Cr-0.08Ti-0.02Fe (wt. %). Details of the thermomechanical processing of the alloy are described elsewhere [5]. Briefly, the alloy was homogenized at 500 °C for 24 h, hot rolled (~400 °C), subjected to solution heat treatment at 500 °C for 1 h and water-quenched. Parts of the samples were produced in flat 'dog-bone' shape to perform a cold pre-deformation by stretching to a residual plastic strain of ~3%. Un-deformed and 3% pre-deformed states were called as 'undef' and '3%-def', respectively. Finally, all samples were aged at 170 °C for different ageing times in a range from 0.25 to 96 h.

2.2. Mechanical tests

To characterize a general mechanical behavior of the alloy during aging, hardness measurements were conducted using a Wilson Wolpert 402 MVD hardness tester at a constant load of 5 N and a loading time of 15 s. Average hardness values and standard deviation were obtained using at least ten indentations in arbitrarily selected areas for each condition.

Tensile tests were performed for each alloy in points chosen on the basis of age-hardening response. The yield stress (YS), the ultimate tensile strength (UTS) and the elongation-to-fracture (δ) were measured using an Instron 5882 tensile testing machine at an initial strain rate of $\sim 10^{-3}$ s^{-1}. The YS, UTS and δ values were averaged using three samples from each condition.

2.3. TEM analysis

TEM specimens were prepared by standard electropolishing procedure with a solution of 2/3 methanol and 1/3 nitric acid at −30 °C using a Struers TenuPol-5 twin-jet unit. The microstructure of the alloy was characterized at low magnifications using a JEOL JEM-2100F TEM equipped with an JEOL ADF detector. A JEOL ARM-200F microscope operated at 200 kV and equipped with a probe-aberration corrector was used to examine the crystal structure of the precipitates formed in the aged samples. A 0.08 nm probe size with 27 wmrad convergence semi-angle was used to acquire high-resolution ADF-STEM images in representative $\{200\}_{Al}$ projections. STEM images were acquired with a JEOL ADF detector, using an inner collection semi-angle of 35 mrad. Noise with periodicities shorter than ~0.14 nm was reduced in all the ADF-STEM images applying fast Fourier transform (FFT) filtering.

2.4. Modelling and computations

The known crystal structures of various phases belonging to the Al—Cu(-Mg) and Al—Mg—Si(-Cu) alloy systems were used to identify atomic column arrangements in the $\{200\}_{Al}$ projection cross-sections of the rod- and plate-like precipitates. DFT calculations of the formation enthalpies for the hybrid structures were performed at zero Kelvin with the Vienna ab initio Simulation Package (VASP) [17,18] using the Perdew-Burke-Ernzerhof (PBE) gradient approximation [19]. A gamma-centered k-point mesh was used in all calculations with a plane wave energy cut-off above 400 eV and a maximal k-point distance of 0.18 $Å^{-1}$. The Methfessel-Paxton method of 1st order was applied for atomic position relaxations with maximum force of 0.001 eV/Å [20] and a smearing factor of 0.2. For accurate energies, all relaxations were followed by a static calculation using the tetrahedron method with Bloch corrections. The formation enthalpy (ΔH) for the UHP was estimated as [7,21]:

$$\Delta H = E_T - n_{Cu} \times E_{Cu} - n_{Mg} \times E_{Mg} - n_{Si} \times E_{Si} \quad (2)$$

where E_T is the total energy of the supercell with the atomic column arrangements for the suggested variant of the UHP, n_{Cu}, n_{Mg} and n_{Si} are the number of Cu, Mg and Si atoms in this supercell, and, E_{Cu}, E_{Mg} and E_{Si} (or E_X) are the solid solution energies for each Cu, Mg or Si atom in fcc-Al matrix, respectively. The E_X values were calculated as:

$$E_X = E_{Al_{255}X} - 255/256 \times E_{Al_{256}} \quad (3)$$

where $E_{Al_{255}X}$ is the total energy of the supercell due to substitution of one of 256 Al atoms with an X atom (Cu, Mg or Si), $E_{Al_{256}}$ is the total energy of the 256 Al atoms in a *fcc* configuration.

3. Results

3.1. Mechanical characterization

Fig. 1 gives a general picture of the age-hardening response of the alloy in 'undef' and '3%-def' states. Fig. 1a combines results of the hardness measurements and the yield stress evolution to indicate main aging stages (under-, peak- and over-aging) in the alloy. Fig. 1b represents typical engineering stress-strain curves in 'undef' and '3%-def' states. It is seen that an initial fast hardening response and the formation of a short hardness plateau up to 1 h with hardness of ~120 $HV_{0.5}$ takes place in both states. A prolonged aging leads to a gradual increase in hardness/YS up to maximum values of ~170 $HV_{0.5}$/~405 MPa and ~160 $HV_{0.5}$/~390 MPa reached after 16 h and 4 h in the 'undef' and '3%-def' states, respectively. The

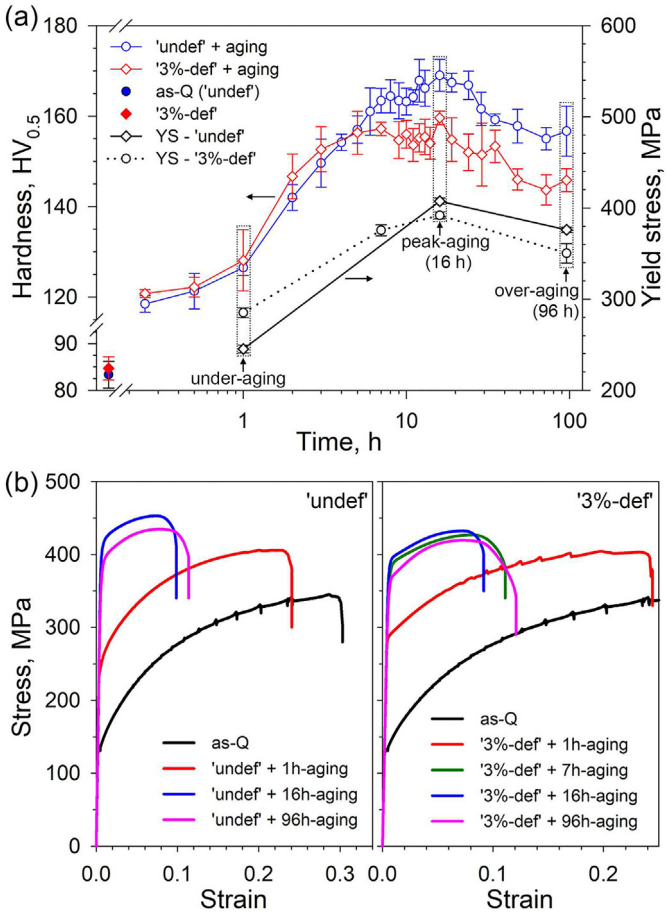

Fig. 1. Age-hardening curves and typical engineering stress-strain curves for the alloy in 'undef' and '3%-def' states followed by aging at 170 °C. Hardness measurements and yield stress evolution are well-agreed with one another depicting the main aging stages in the alloy - under-, peak- and overaging. Aging times - 1, 16 and 96 h indicated by dashed frames were chosen for TEM characterization.

main feature of the '3%-def' state is that the hardness plateau takes place during aging times between 4 and 16 h, whereas the as-quenched state displays a more narrow hardness peak. Thus, it is clear that the 3%-pre-deformed alloy is not able to provide the same strength level as the alloy in 'undef' state after peak-aging.

The following over-aging, associated with hardness loss, occurs at similar rates in both 'undef' and '3%-def' states. Samples after aging for 1, 16 and 96 h are expected to be interesting for analyzing the microstructure and precipitation behavior in under-, peak- and over-aging conditions, respectively. For this reason, they have been chosen for TEM characterization.

3.2. TEM observations

Careful analysis of the precipitate evolution has been performed on the aged 'undef' and '3%-def' states in Ref. [5]. In general, different levels of a precipitate hierarchy can be identified in the alloy: (i) coarse primary particles (not shown here); (ii) dispersoids (not shown here); and (iii) nano-sized precipitates appearing during aging [5]. Representative ADF-STEM and DF-TEM images, showing a typical morphology and distribution of the latter in the 'undef' and '3%-def' samples after peak-aging, are given in Fig. 2a and b, respectively.

The precipitates appearing during aging could be divided to two different groups depending on their localization. The first group is associated with precipitates formed in dislocation-free regions. They are discrete rod- and plate-/lath-like usually inter-grown with each other forming hybrid-type precipitates (Fig. 2). The second group of precipitates forms continuous and somewhat jagged bands along dislocation lines and loops (Fig. 2). It has been shown [5] that these precipitates also are hybrid-type, comprising the β″, β′-Cu, L, C, and Q′-phase fragments depending on aging stage.

It is worthy to note that dislocations can naturally occur in the 'undef' state, where they are non-uniformly distributed in the matrix and predominantly observed in regions close to grain boundaries, coarse primary particles and dispersoids. It was also shown [5] that there is no difference in the precipitate crystal structure evolution in dislocation-free regions or at dislocation lines in the 'undef' and '3%-def' samples. For this reason, we do not pay our attention to a separate characterization of the hybrid precipitates in these regions.

Among all the precipitate crystal structures presented also in Ref. [5], one UHP quite frequently observed in the alloy after aging for different times is shown in Fig. 3. This UHP, having discrete rod morphology along $\langle 100 \rangle_{Al}$, is characterized by certain atomic column arrangements in the core and in the lateral interfaces as

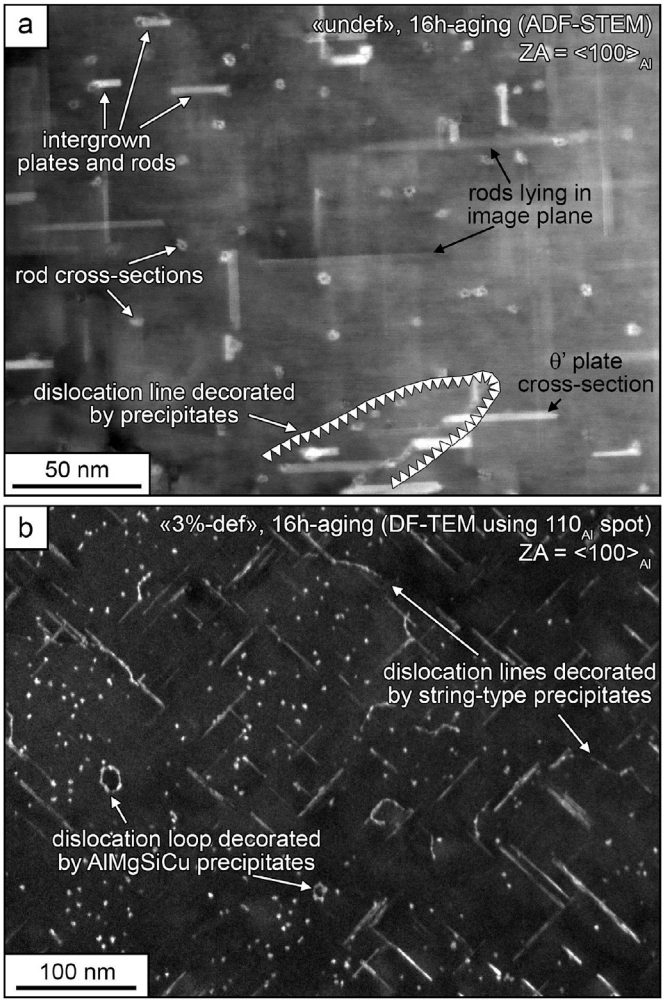

Fig. 2. ADF-STEM (a) and DF-TEM images (b) showing the typical microstructure of the 'undef' and '3%-def' samples in peak-aging conditions, respectively. Bright spots and lines in ADF-STEM/DF-TEM images represent rod and plate cross-sections corresponding to the AlMgSiCu-type precipitates and θ′ plates, respectively, which are normal to the image plane. Grey diffuse lines are rod-like precipitates lying in the image plane. Precipitate inter-grown cases are also marked.

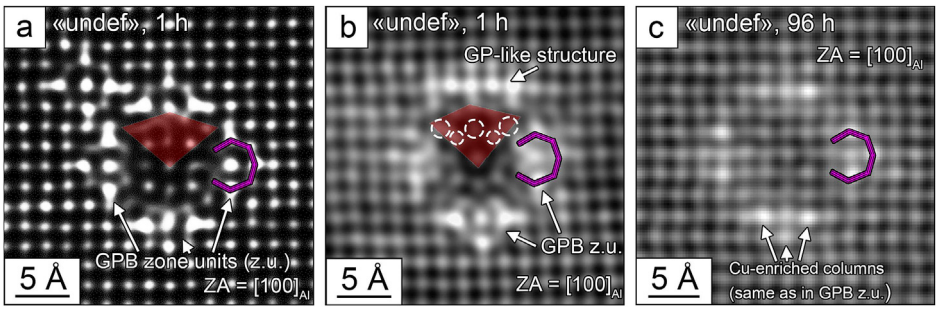

Fig. 3. ADF-STEM images of the UHP in the alloy aged for 1 h (a,b) and 96 h (c). Typically this structure has a 4-fold symmetry of its atomic column arrangement in the core. The quadrant of the repeating structural element is marked by a red area. The distribution of atomic columns in the surrounding regions is typical for the GPB zone units (marked by purple lines). This UHP structure has been found connecting with monoatomic Cu layers in fcc-Al matrix (GP-like structures) (b) and overlapped by Al matrix (c), in this case only Cu column distributions typical for the GBP zone units can be identified. (For interpretation of the references to colour in this figure legend, the reader is referred to the Web version of this article.)

observed in cross-section in $\{200\}_{Al}$ projections. The internal (core) region resembles the structure of a single fragment of the β″-phase of the Al–Mg–Si system – the previously described β″-eye [5,15,16,22], while the lateral surface is composed of four GPB zone unit pillars from the Al–Cu–Mg system [8] (Fig. 3a). It is worthy to note that this hybrid precipitate also can be found as a discrete precipitate where at least three lateral sides of the rods can be occupied by the GPB zone units, and one side by the GP-like structures (monoatomic Cu layer in fcc-Al matrix) as shown in Fig. 3b. This type of discrete precipitate, observed in all the under-, peak- and over-aging states of the Al–Cu–Mg–Si alloy, demonstrates a relatively high thermal stability during aging at elevated temperatures.

In addition to being observed as a discrete precipitate, the UHP has been found as a part of hybrid precipitate complexes as intergrown with θ' plates and with other AlMgSiCu-type precipitates, see Fig. 4a–b and c, respectively. In this case, only a certain fragment of the UHP is present as marked by red areas in Fig. 4. It should be noted that all the hybrid AlMgSiCu-type precipitates are found to be connected to at least one UHP fragment in the alloy. The UHP fragments inter-grown to other precipitate types (Fig. 4) are more frequently observed than the discrete UHP rods in bulk matrix (Fig. 3).

It is also seen in Fig. 4a and shown in Ref. [5] that other AlMgSiCu-type precipitates can form at the edge of semi-coherent interfaces of the θ′-phase plates containing different types of faults described in detail in Ref. [23].

3.3. DFT calculations

The cross-section of the UHP experimentally found in the present work is shown in Fig. 5, together with several atomic models suggested using the phase construction rules based on the column arrangement principles [15]. Elements occupying certain atomic

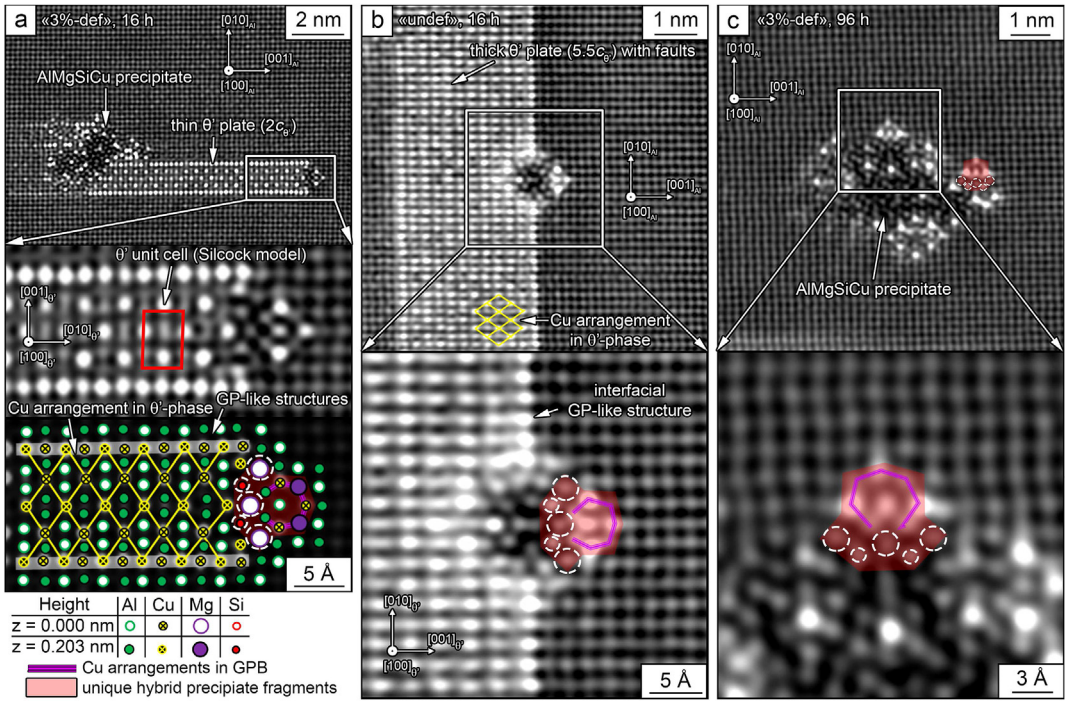

Fig. 4. Well-defined fragments of the UHP (marked by red areas) interacting with the θ′ plate edges (a), broad interface of a θ′ plate (b) and a AlMgCuSi precipitate (c) in the Al–Cu–Mg–Si alloy in 'undef' (b) and '3%-def' states (a,c) followed by aging for 16 h (a,b) and 96 h (c). The thick θ′ plate contains different types of stacking faults described in detail in Ref. [24]. (For interpretation of the references to colour in this figure legend, the reader is referred to the Web version of this article.)

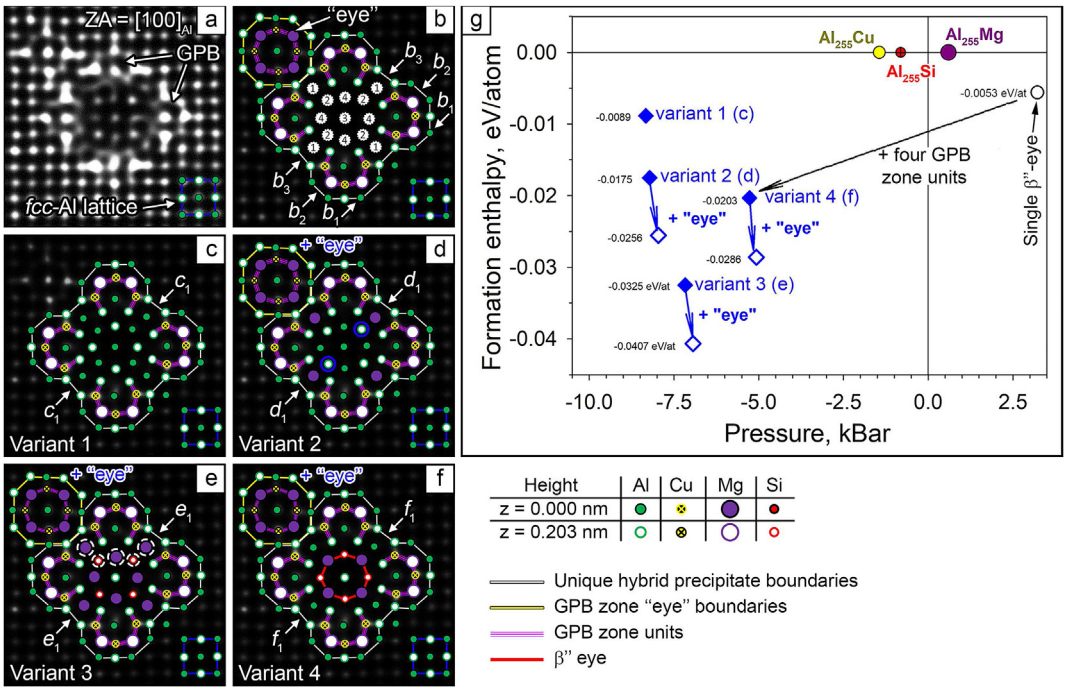

Fig. 5. Results of DFT calculations showing the formation enthalpy (eV per atom in a supercell) for several variants of the atomic column arrangements suggested for the UHP structure (a). The external/shell structure is composed from four GPB zone units (b). ZA is a zone axis of fcc-Al matrix. Because of the 4-fold symmetry of the internal crystal structure, four types of the columns (1–4 sites) occupied by different elements can be identified. The phase construction rules given in work [15] were used to build four variants of the unique hybrid precipitate structure (c–f). b_2-b_2, … ,f_1-f_1 lines are presented to identify positions of the line defects considered as a 0.5 × a_{Al} shift along $[100]_{Al}$ direction of the atomic columns (marked by the blue circles as an example in (d)) in comparison with the ideal fcc-Al, where the atomic columns have the same 'height' (b_1-b_1 line). This line defect ordering was used to explain the formation of the GPB zone unit [8] and β″-phase [15]. Pressure levels due to substitution of one atom column of Al with Cu, Mg or Si in supercell of 256 Al atoms in a *fcc* configuration as well as the formation enthalpy for the single β″-eye in the fcc-Al lattice are represented. (For interpretation of the references to colour in this figure legend, the reader is referred to the Web version of this article.)

columns were determined by counting the number of NNs [15]. The same mechanism was used to explain of the GPB zone unit and β″-eye structures formation as line defects (LDs) ordering in $\langle 100\rangle_{Al}$ directions by Kovarik et al. [8] and Andersen et al. [15], respectively. These LDs can be described as a segment of a $[100]_{Al}$ atomic column undergoing a 0.5 × a_{Al} shift (0.5 × 0.405 nm) in an fcc-Al lattice along the main axis of the forming rod-like precipitate [8,15]. This shift decomposes the fcc-Al lattice into columns with atoms of different NNs providing caches for smaller atoms (for example, Si and Cu) and larger atoms (Mg) and is a strain-alleviation mechanism [15]. The LDs can be easily identified in (Fig. 5b) as Al atomic columns having the same height along the b_1-b_1 line in the ideal fcc-Al matrix, and on a contrary, changing the atomic column height along b_2-b_2 line corresponding to the GPB zone formation. Potential positions of the line defects can easily be identified in the UHP core along b_3-b_3 line (sites 1–3) and site 4 in addition, in Fig. 5b.

Regarding the internal structures suggested for the UHP imaged in Fig. 5a, Variant 1 shown in Fig. 5c has no LDs along the c_1-c_1 line and Al atoms should occupy all internal (core) columns in the $\{200\}_{Al}$ projections in accordance with the phase construction rules. The $[100]_{Al}$ LDs occupy sites 2 along d_1-d_1 and sites 4 in Variant 2 (Fig. 5d); sites 2 and 3 along e_1-e_1 and site 4 (Mg) in Variant 3 (Fig. 5e); and site 3 along f_1-f_1 in Variant 4 (Fig. 5f). These $[100]_{Al}$ LDs arrangements aid solute decomposition by partitioning the fcc-Al matrix locally into columns occupied by one sort of elements [15] – Al columns in Variant 2; Si, Al and Mg in Variant 3; and Al in Variant 4, respectively. With these LD orderings, Variant 3 is the most defective structure among the suggested atomic models compared to an ideal fcc-Al structure. It should be noted that the atomic column arrangement in Variant 4 has structural similarities with the 'building' blocks of the β″-phase [5,15,16,22] – the β″-eye marked with a red line in Fig. 5f.

To verify experimentally the observed structures, DFT calculations have been performed using suggested variants of the UHP models showing, in general, a 4-fold symmetry, as well as consisting of the additional GPB zone 'eye' marked by the closed yellow line in Fig. 5b and d-f. It should be noted that distribution and heights of the Al columns along the UHP/'eye' (GPB zone) and UHP/fcc-Al matrix interfaces are similar, thus, exclusion of the GPB 'eye' (marked by the yellow line in Fig. 5) from the supercell model is possible and the phase construction rules are fulfilled.

The formation enthalpies calculated are presented in Fig. 5g. It is seen that the formation enthalpy changes by −8.4 meV/at due to the incorporation of the GPB zone 'eye' into Variants 2–4 of the suggested UHP structures. The formation of this GPB zone 'eye' in the fcc-Al matrix seems more favorable than the single β″-eye in the same conditions (−5.3 meV/at). The difference in formation enthalpy of ~3 meV/at for both structures is however quite small. It has been suggested [21] that this small difference could easily be reversed by taking into account effects which have been ignored in the DFT calculations. Despite of this the UHP in accordance with the model of Variant 3 tends to have the lowest formation enthalpy among the four variants suggested in the present work.

4. Discussion

4.1. Stability of the UHP structure

Analysis of ADF-STEM images revealed that the UHP can be frequently found in all investigated conditions of the Al–Cu–Mg–Si alloy. An example of this discrete rod-like UHP

structure, presented in Fig. 3a, was used to reconstruct its crystal structure. Several atomic models of the rod-shaped UHP, shown in Fig. 5, were suggested using the phase construction rules [15]. The DFT calculations applied for the suggested variants of the UHP structure shows that the model of Variant 3 (Fig. 5e) is most energetically favorable. This model comprises a core with local 4-fold symmetry surrounded by GPB zone unit pillars. The core structure of the UHP can be represented as the β″-eye rotated by 45° compared with the 'conventional' orientation of 'building' blocks of the β″-phase relative to the Al matrix. The stoichiometric composition of the UHP (Variant 3 with the four GPB zone units and excluding the additional GPB zone 'eye') is $Al_{13}Cu_{12}Mg_{16}Si_4$. TEM results show that substitutions of the GPB zone units are also possible by monoatomic GP-like structures (Fig. 3b).

Additional DFT calculations show that the formation of GPB zone 'eye' in fcc-Al matrix (−8.4 meV/at on average) is probably more favorable than the single β″-eye in the same conditions (−5.3 meV/at). The difference in formation enthalpy of ~3 meV/at for both structures is however quite small. It has been suggested [21] that this small difference could easily be reversed by taking into account effects which have been ignored in DFT calculations. However, in general, incorporation of the GPB zone 'eye' to all the suggested variants of the UHP structures reduces the total formation enthalpy. It is interesting to note that the attempt to simulate the model comprising a UHP core (Variant 3) surrounded only by fcc-Al matrix causes a failure to comply with the phase construction rules and will increase the energy of the system.

Careful analysis of the TEM images presented by Wenner et al. [25] shows that the atomic column arrangements similar to the UHP structure can also be found in an Al-4.0Zn-2.0Cu-1.0Mg-0.70Si-0.55Mn-0.20Fe (wt. %) alloy after aging at 150 °C for 32 days as shown in Fig. 6. Observations of this UHP in the Al–Zn–Cu–Mg–Si alloy indicates that Cu, Mg and Si additions play an important role in the formation of such type of precipitate fragments. It seems that this precipitate can be found in a broad range of chemical compositions of commercial alloys containing Cu, Mg and Si.

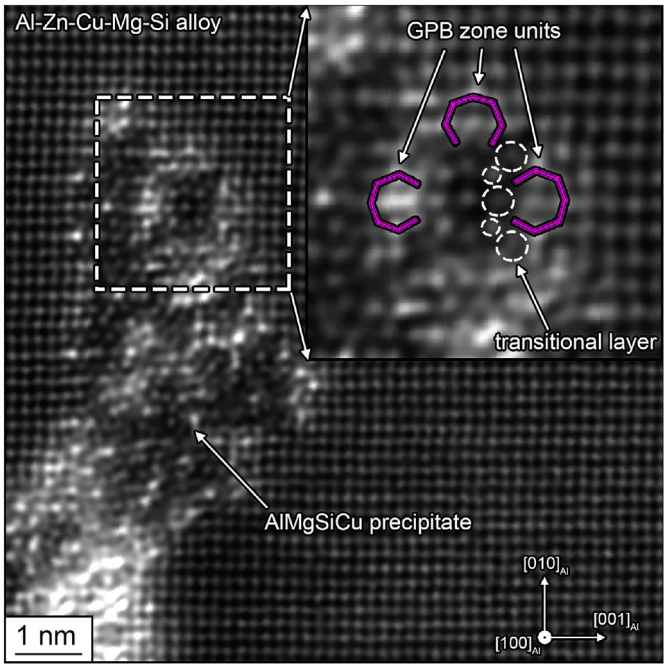

Fig. 6. An ADF-STEM image extracted from Ref. [25] and modified to show the presence of the UHP in the Al-4.0Zn-2.0Cu-1.0Mg-0.70Si-0.55Mn-0.20Fe (wt. %) alloy after aging at 150 °C for 32 days.

4.2. Fragmentation of the UHP

Analysis of the precipitate formation shows that phases found in the Al–Cu–Mg–Si alloy in under-, peak- and over-aging states are very diverse. The main characteristic of this process is the intense fragmentation of the crystal structures of well-known phases and formation of hybrid precipitates. They consist of a number of different metastable phases belonging to the Al–Cu (θ″- and θ′-phases, GP-like structures), Al–Cu–Mg (GPB zone units) and Al–Mg–Si–Cu systems (β″, β′-Cu, Q′, C and C1-phases, as well as disordered structures consisting of the hexagonal Si-network in $\{100\}_{Al}$ projections) [5]. A similar fragmentation behavior was observed for the UHP found in the present alloy. Examples of the complex precipitates involving the UHP fragment are shown in Fig. 4. In this case only one GPB zone unit and atomic columns of one quadrant (marked by red areas in Fig. 3a and b) can be observed in the external/shell structures and in the core, respectively.

It seems like these tiny fragments of the UHP incorporated into other precipitates make the crystal structures of other precipitates compatible with the fcc-Al matrix and play an important role in the stabilization of such hybrid structures. In other words, the Si and Mg columns in the crystal configuration present in this unique fragment (marked by the dashed circles in Figs. 3b and 4) contribute to reducing the misfit strain at precipitate interfaces. It can be supposed that a certain level of distortion is required to reduce the mismatch between the fcc-Al matrix and precipitates. This distortion level is provided by close, but opposite values of the pressures originating from infinite Si and Mg columns embedded to the fcc-Al matrix and parallel to the $\langle 100\rangle_{Al}$ directions. These pressures calculated by DFT and presented in Fig. 5g (marked as $Al_{255}Si$ and $Al_{255}Mg$) appear in supercells despite the fact that Mg and Si atoms have the biggest differences in atom sizes among main alloying elements - Cu (r_{Cu} = 1.28 Å), Mg (r_{Mg} = 1.60 Å) and Si (r_{Si} = 1.17 Å) from Al (r_{Al} = 1.43 Å) [24].

Concerning the interaction between the θ′-phase plates and UHP fragments, this fragment can also be found on semi-coherent edges of thin θ′-phase plates with thickness of $2c_\theta$ (Fig. 4a) [14], and on broad coherent interfaces of the thick θ′-phase (Fig. 4b) [5,11]. It is seen in Fig. 4a and shown in Ref. [5] that other AlMgSiCu-type precipitates can also be formed at edge semi-coherent interfaces of thin and thick θ′-phase plates containing different types of faults as described in detail in Ref. [23].

4.3. Effect of the UHP formation on mechanical properties

Effect of the UHP formation on mechanical properties in the Al–Cu–Mg–Si alloys is not obvious in a framework of this study. In earlier work [5] the negative effect of pre-deformation (in '3%-def' state) on the peak hardness values was found and associated with enhanced density of dislocations. The deformation initiates heterogeneous nucleation and accelerates the kinetics of phase transformations and growth of the AlMgSiCu precipitates (β″, β′-Cu, C and Q′) in comparison with the AlCu-type (θ″ and θ′) and AlCuMg-type (S1) precipitates. This leads to shift in time scale the maximum strengthening contributions originating from the different types of precipitate. It happens despite a high level hybridization between the phases belonging to different alloying systems.

The UHP structure is only one particular case of atom column arrangements among several changes in precipitation behavior taking place in Al–Cu alloys due to small Mg and Si additions [1–5,15,21]. Thus, the UHP and its fragments influence cannot itself be directly related to mechanical properties during aging because

of the 'extreme' hybridization present in the precipitates observed in Al−Cu−Mg−Si alloys.

The effect of the phase hybridization can be interesting in microstructural design aspects of commercial Al alloys containing Cu, Mg and Si. Firstly, it can affect the dislocation-precipitate interaction due to its influence the strain surrounding precipitates causing a change in the precipitate strengthening contribution to the overall strength of these alloys. In addition, an 'extra' energy can be required for a dislocation to cut a hybrid precipitate comprising from the different phase fragments having incompatible slip systems in comparison with the single-phase precipitate. Moreover, the phase hybridization can enhance precipitate dispersion in the case of heterogeneous nucleation with the effect on macroscopic mechanical properties of the alloy. Finally, some of the inter-grown phases may be more stable than others, which can improve the thermal stability of whole precipitate complexes with a positive effect on the heat resistance of these alloys. An evidence of improving stability of the phase fragments can be given by our current observations of the GPB zone units inter-grown with other types of precipitates in the alloy after over-aging, despite their metastable nature in Al−Cu−Mg alloys [5].

5. Conclusions

Precipitate behavior in an Al-4.9Cu-0.74Mg-0.51Si–0.48Mn-0.1Cr-0.08Ti-0.02Fe alloy (in wt. %) has been investigated during ageing at 170 °C. A new UHP crystal structure has been identified in ADF-STEM images in $\{100\}_{Al}$ projections. This precipitate-type consists of rod-like discrete particles along $\langle 100\rangle_{Al}$ in the fcc-Al matrix, and its fragments can interact with other hybrid AlMgSiCu-type precipitates and θ′-phase plates. DFT calculations performed on a discrete rod-like UHP having local 4-fold symmetry show that its most stable internal atomic configuration is composed of alternating Mg and Si columns forming a transitional layer that provides a good match between the fcc-Al matrix and external layers (along the lateral surface of the rod) consisting of GPB zone units and/or GP-like structures. This configuration of Mg and Si columns stabilizes the phase fragments in the UHP structure.

Funding

This work was financially supported by the Faculty of Natural Sciences at the Norwegian University of Science and Technology (NTNU), Norway, Project No. 81617879 and the Ministry of Education and Science of the Russian Federation, Russia, under the Agreement No. 14.584.21.0023 (ID number RFMEFI58417X0023). The authors acknowledge support from The Research Council of Norway (NFR), and industrial partners through the following projects 247783, 247598 and 237885. The TEM work was carried out on the NORTEM infrastructure (NFR 197405) at the TEM Gemini Centre, Trondheim, Norway. The DFT calculations were performed on resources provided by UNINETT Sigma2 - the National Infrastructure for High Performance Computing and Data Storage in Norway.

CRediT authorship contribution statement

Marat Gazizov: Investigation, Methodology, Writing - original draft, Visualization. **Calin Daniel Marioara:** Investigation, Data curation, Methodology, Writing - review & editing. **Jesper Friis:** Software, Methodology, Writing - review & editing. **Sigurd Wenner:** Writing - review & editing. **Randi Holmestad:** Resources, Writing - review & editing, Supervision. **Rustam Kaibyshev:** Resources, Writing - review & editing.

Acknowledgment

The authors are grateful to the staff of the TEM Gemini Center at NTNU and the Joint Research Center at Belgorod State University for their assistance with the structural and mechanical characterizations.

References

[1] I. Polmear, Light Alloys: from Traditional Alloys to Nanocrystals, third ed. Edition, Butterworth-Heinemann/Elsevier, Oxford (UK), 2006.
[2] D.G. Eskin, Decomposition of supersaturated solid solutions in Al-Cu-Mg-Si alloys, J. Mater. Sci. 38 (2003) 279−290, https://doi.org/10.1023/A:1021109514892.
[3] M.R. Gazizov, A.V. Dubina, D.A. Zhemchuzhnikova, R.O. Kaibyshev, Effect of equal-channel angular pressing and aging on the microstructure and mechanical properties of an Al-Cu-Mg-Si alloy, Phys. Met. Metallogr. 116 (7) (2015) 718−729, https://doi.org/10.1134/s0031918x15070066.
[4] L. Liu, J.H. Chen, S.B. Wang, C.H. Liu, S.S. Yang, C.L. Wu, The effect of Si on precipitation in Al-Cu-Mg alloy with a high Cu/Mg ratio, Mater. Sci. Eng., A 606 (2014) 187−195, https://doi.org/10.1016/J.MSEA.2014.03.079.
[5] M. Gazizov, C.D. Marioara, J. Friis, S. Wenner, R. Holmestad, R. Kaibyshev, Precipitation behavior in an Al-Cu-Mg-Si alloy during ageing, Mater. Sci. Eng. 767 (2019), 138369, https://doi.org/10.1016/J.MSEA.2019.138369.
[6] D.A. Porter, K.E. Easterling, M.Y. Sherif, Phase Transformations in Metals and Alloys, third ed. Edition, CRC press, New York, 2014.
[7] L. Kovarik, M.J. Mills, Ab initio analysis of Guinier-Preston-Bagaryatsky zone nucleation in Al-Cu-Mg alloys, Acta Mater. 60 (9) (2012) 3861−3872, https://doi.org/10.1016/j.actamat.2012.03.044.
[8] L. Kovarik, S.A. Court, H.L. Fraser, M.J. Mills, GPB zones and composite GPB/GPBII zones in Al-Cu-Mg alloys, Acta Mater. 56 (17) (2008) 4804−4815, https://doi.org/10.1016/j.actamat.2008.05.042.
[9] D. Vaughan, J.M. Silcock, The orientation and shape of θ precipitates formed in an Al-Cu alloy, Phys. Status Solidi 20 (2) (1967) 725−736, https://doi.org/10.1002/pssb.19670200235.
[10] C.D. Marioara, S.J. Andersen, T.N. Stene, H. Hasting, J. Walmsley, A.T.J. Van Helvoort, R. Holmestad, The effect of Cu on precipitation in Al-Mg-Si alloys, Phil. Mag. 87 (23) (2007) 3385−3413, https://doi.org/10.1080/14786430701287377.
[11] L. Bourgeois, C. Dwyer, M. Weyland, J.-F. Nie, B. Muddle, Structure and energetics of the coherent interface between the θ' precipitate phase and aluminium in Al-Cu, Acta Mater. 59 (18) (2011) 7043−7050, https://doi.org/10.1016/j.actamat.2011.07.059.
[12] M. Fiawoo, X. Gao, L. Bourgeois, N. Parson, X.Q. Zhang, M. Couper, J.F. Nie, Formation of multiple orientation relationships of Q precipitates in Al-Mg-Si-Cu alloys, Scripta Mater. 88 (2014) 53−56, https://doi.org/10.1016/j.scriptamat.2014.05.013.
[13] T. Saito, F.J.H. Ehlers, W. Lefebvre, D. Hernandez-Maldonado, R. Bjørge, C. Marioara, S. Andersen, E. Mørtsell, R. Holmestad, Cu atoms suppress misfit dislocations at the β"/Al interface in Al-Mg-Si alloys, Scripta Mater. 110 (2016) 6−9, https://doi.org/10.1016/j.scriptmat.2015.07.033.
[14] A. Biswas, D.J. Siegel, C. Wolverton, D.N. Seidman, Precipitates in Al-Cu alloys revisited: atom-probe tomographic experiments and first-principles calculations of compositional evolution and interfacial segregation, Acta Mater. 59 (15) (2011) 6187−6204, https://doi.org/10.1016/J.ACTAMAT.2011.06.036.
[15] S.J. Andersen, C.D. Marioara, J. Friis, R. Bjørge, Q. Du, I.G. Ringdalen, S. Wenner, E.A. Mørtsell, R. Holmestad, T. Saito, J. Røyset, O. Reiso, Directionality and column arrangement principles of precipitates in Al-Mg-Si-(Cu) and Al-Mg-Cu linked to line defect in Al, Mater. Sci. Forum 877 (2016) 461−470. https://doi.org/10.4028/www.scientific.net/MSF.877.461.
[16] T. Saito, E.A. Mørtsell, S. Wenner, C.D. Marioara, S.J. Andersen, J. Friis, K. Matsuda, R. Holmestad, Atomic structures of precipitates in Al-Mg-Si alloys with small additions of other elements, Adv. Eng. Mater. 20 (7) (2018), https://doi.org/10.1002/adem.201800125, 1800125.
[17] G. Kresse, J. Hafner, Ab initio molecular dynamics for open-shell transition metals, Phys. Rev. B 48 (17) (1993) 13115−13118, https://doi.org/10.1103/PhysRevB.48.13115.
[18] G. Kresse, D. Joubert, From ultrasoft pseudopotentials to the projector augmented-wave method, Phys. Rev. B 59 (3) (1999) 11−19, https://doi.org/10.1103/PhysRevB.59.1758.
[19] J.P. Perdew, K. Burke, M. Ernzerhof, Generalized gradient approximation made simple, Phys. Rev. Lett. 78 (1997), https://doi.org/10.1103/PhysRevLett.78.1396, 1396−1396.
[20] M. Methfessel, A.T. Paxton, High-precision sampling for Brillouin-zone integration in metals, Phys. Rev. B 40 (6) (1989) 3616−3621, https://doi.org/10.1103/PhysRevB.40.3616.
[21] S. Wenner, J. Friis, C.D. Marioara, R. Holmestad, Precipitation in a mixed Al-Cu-Mg/Al-Zn-Mg alloy system, J. Alloys Compd. 684 (2016) 195−200, https://doi.org/10.1016/j.jallcom.2016.05.132.
[22] M.A. van Huis, J.H. Chen, M.H.F. Sluiter, H.W. Zandbergen, Phase stability and structural featu res of matrix-embedded hardening precipitates in Al-Mg-Si alloys in the early stages of evolution, Acta Mater. 55 (6) (2007)

2183–2199, https://doi.org/10.1016/J.ACTAMAT.2006.11.019.
[23] S. Wenner, J. Friis, C.D. Marioara, S.J. Andersen, R. Holmestad, Structural modifications and electron beam damage in aluminium alloy precipitate θ'-Al2Cu, Phil. Mag. 95 (31) (2015) 3524–3534, https://doi.org/10.1080/14786435.2015.1090639.
[24] M. Spittel, T. Spittel, Part 3: Non-ferrous Alloys - Heavy Metals, Springer, 2019, https://doi.org/10.1007/978-3-642-14174-4.
[25] S. Wenner, C.D. Marioara, S.J. Andersen, M. Ervik, R. Holmestad, A hybrid aluminium alloy and its zoo of interacting nano-precipitates, Mater. Char. 106 (2015) 226–231, https://doi.org/10.1016/j.matchar.2015.06.002.